Highly Stable and Tunable Chemical Doping of Multilayer WS2 Field Effect Transistor: Reduction in Contact Resistance

ARTICLE *in* ACS APPLIED MATERIALS & INTERFACES · OCTOBER 2015

Impact Factor: 6.72 · DOI: 10.1021/acsami.5b06825

4 AUTHORS, INCLUDING:

Hafiz M W Khalil

Sejong University

6 PUBLICATIONS **0** CITATIONS

SEE PROFILE

Muhammad Farooq Khan

Sejong University

15 PUBLICATIONS **18** CITATIONS

SEE PROFILE

Jonghwa Eom

Sejong University

117 PUBLICATIONS **840** CITATIONS

SEE PROFILE

ACS APPLIED MATERIALS & INTERFACES

Research Article

www.acsami.org

Highly Stable and Tunable Chemical Doping of Multilayer WS_2 Field Effect Transistor: Reduction in Contact Resistance

Hafiz M. W. Khalil, Muhammad Farooq Khan, Jonghwa Eom, and Hwayong Noh*

Department of Physics and Graphene Research Institute, Sejong University, Seoul 143-747, Korea

Supporting Information

ABSTRACT: The development of low resistance contacts to 2D transition-metal dichalcogenides (TMDs) is still a big challenge for the future generation field effect transistors (FETs) and optoelectronic devices. Here, we report a chemical doping technique to achieve low contact resistance by keeping the intrinsic properties of few layers WS_2. The transfer length method has been used to investigate the effect of chemical doping on contact resistance. After doping, the contact resistance (R_c) of multilayer (ML) WS_2 has been reduced to 0.9 kΩ·μm. The significant reduction of the R_c is mainly due to the high electron doping density, thus a reduction in Schottky barrier height, which limits the device performance. The threshold voltage of ML-WS_2 FETs confirms a negative shift upon the chemical doping, as further confirmed from the positions of E^1_{2g} and A_{1g} peaks in Raman spectra. The n-doped samples possess a high drain current of 65 μA/μm, with an on/off ratio of 1.05×10^6 and a field effect mobility of 34.7 $cm^2/(V{\cdot}s)$ at room temperature. Furthermore, the photoelectric properties of doped WS_2 flakes were also measured under deep ultraviolet light. The potential of using LiF doping in contact engineering of TMDs opens new ways to improve the device performance.

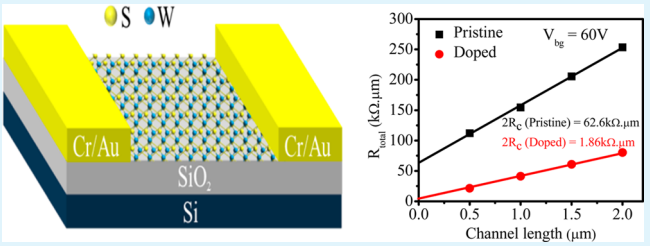

KEYWORDS: *WS_2, TMDs, TLM, contact resistance, Schottky barrier, DUV*

1. INTRODUCTION

In recent years, graphene has attracted much attention due to its significant electrical, optical, and mechanical properties.[1−3] Though graphene has shown an exceptionally high carrier mobility of up to 10^6 $cm^2/V{\cdot}s$,[4,5] its zero band gap prohibits its use in nanoelectronics and optoelectronics. On the other hand, 2D TMD materials like MoS_2 and WS_2 possess reasonable band gaps around 1−2 eV[6,7] and reasonable carrier mobilities.[8,9] WS_2, one of the promising TMD materials, has been widely used as the channel material of the field effect transistors with a large on/off ratio and high field effect mobility.[10,11] Recently, efforts were made to improve the device performance through understanding the influence of contact electrode, limitations in carrier transport, and effect of different substrates on charge carrier mobility.[8,9,12−19] Analysis of the literature reveals that variations in mobility values may came from the Schottky barriers (SBs) at metal/semiconductor interfaces and differences in the fabrication process. In order to overcome the Schottky barrier problem, different strategies have been used. For example, metals such as Al,[13,20] Ni,[14,21,22] Pt,[13,14] Mo,[23] and Au[13,24] have been used to reduce the Schottky barrier. Although some of the reports showed good results, overall contact resistance is still reasonably high due to the internal resistance of the semiconductor. In general, it is very difficult to achieve low contact resistance in WS_2 by simply using the low work function metals because the charge neutrality level (CNL) is located in the center of the band gap.[25,26]

Another possible way to reduce the contact resistance on the metal semiconductor interface is to heavily dope the semiconductor under metals.[27] After heavy doping, the effective Schottky barrier height becomes small and electrons can easily tunnel through the barrier. Applying the traditional ion implanted doping method to 2D materials is not straightforward due to their atomically thin body nature. On the other hand, surface modification by molecules or ions shows the great advantages over ion implantations when applied to the 2D materials. There are a number of reports on the chemical doping of 2D layered materials including PEI molecular doping in MoS_2[28] and potassium doping in WSe_2 and MoS_2.[29] Those studies shows limited reduction in contact resistance and also have long-term stability issues. Controlled chemical doping of multilayer WS_2 and their photoelectrical properties are not well-explored in the community.

In this paper, we report the n-doping of WS_2 with lithium fluoride (LiF). LiF is a widely used n-dopant for the organic semiconductor industry due to its strong electron-donating ability. After doping, we observe a large reduction in contact resistance. Raman spectroscopy and transport measurement were carried out to confirm that LiF imposes the n-doping in WS_2. The doped-multilayer WS_2 device shows excellent field effect properties with a drain current of 65 μA/μm, an I_{on}/I_{off} of 1.05×10^6, and a field effect mobility of 34.7 $cm^{-2}/V{\cdot}s$. Lastly, the effect of doping on photocurrent response was studied by irradiation of deep ultraviolet (DUV) light. The results indicate

Received: July 27, 2015
Accepted: October 5, 2015

DOI: 10.1021/acsami.5b06825
ACS Appl. Mater. Interfaces XXXX, XXX, XXX−XXX

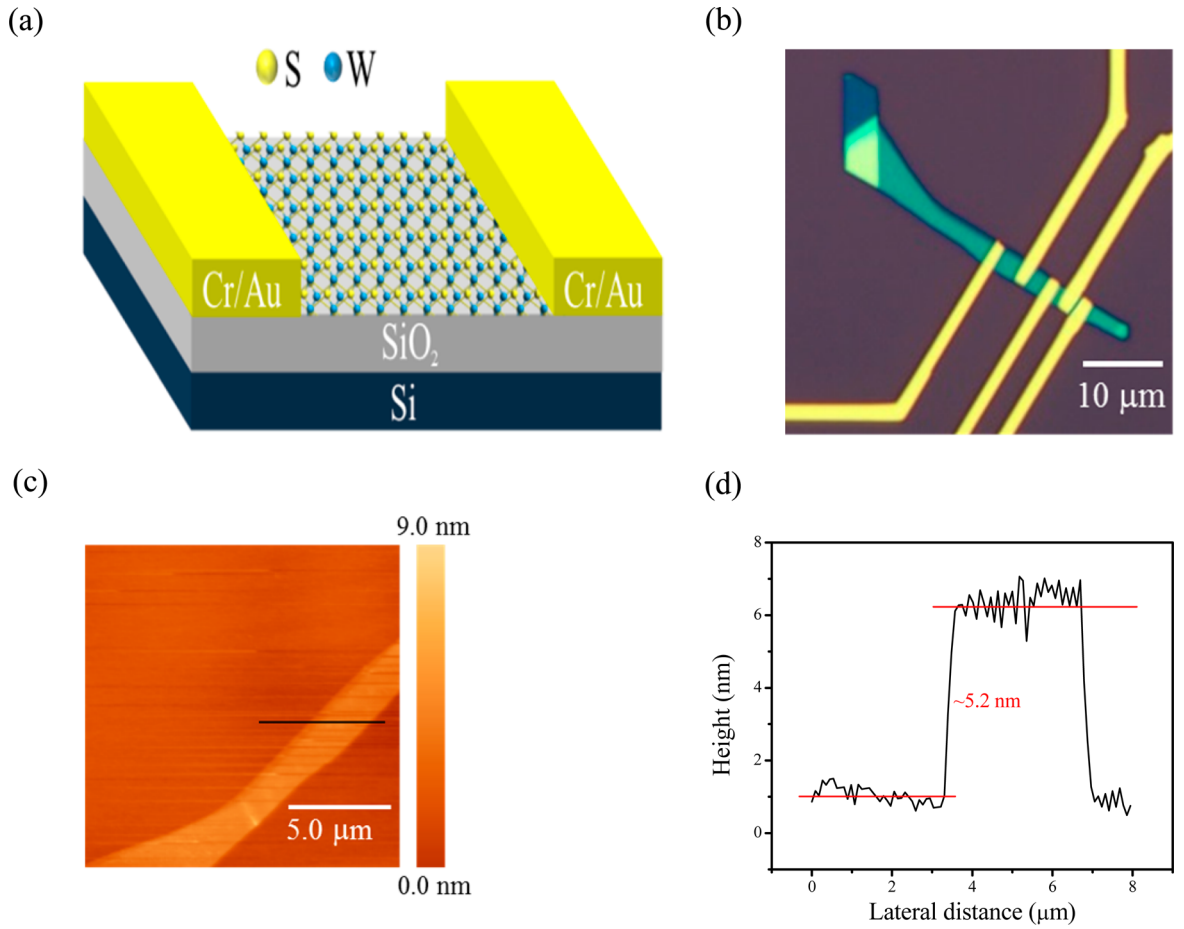

Figure 1. (a) Schematic of the back gated WS_2 FET. Heavily p-doped silicon is used as the back gate and 300 nm SiO_2 as back gate dielectric. Cr/Au is used as source−drain contact. (b) Optical image of ML-WS_2 device. Scale bar is 10 μm. (c) Atomic force microscope (AFM) image of the device shown in (b). (d) Height profile of the ML-WS_2 film obtained at the location of the black line in (c).

that this doping technique can also be applied to other TMD materials to reduce the contact resistance.

2. EXPERIMENTAL SECTION

The WS_2 flakes were mechanically exfoliated from a bulk ingot purchased from HQ graphene by the scotch tape method and then transferred to a heavily p-doped silicon substrate with a 300 nm SiO_2 capping layer. After the transfer of a flake onto the Si substrate, photolithography was used to make the large electrode pattern with Cr/Au (5/30 nm) film that was deposited using the thermal evaporator and lift-off technique. The thickness of WS_2 flakes was examined using an optical microscope and Raman spectroscopy, and then confirmed by atomic force microscopy (AFM). Raman spectra were obtained with a Renishaw Raman spectrometer with an excitation of 514 nm and a low laser power of 1 mW with a 30 s integral time was used to avoid any heating effect. Electron beam lithography was used to define the source−drain contact with a fixed width of 1 μm, followed by evaporation of Cr/Au (8/60 nm) film with a thermal evaporator under a vacuum of 2×10^{-6} Torr at room temperature. Structures for transfer length method (TLM) were designed with channel lengths of 0.5, 1, 1.5, and 2 μm to extract the contact resistance. The electrical measurements were carried out using a Keithley 2400 source meter and Keithley 6485 picoammeter at room temperature in vacuum. To dope the device after initial measurements, the WS_2 FET device was soaked in LiF solution at room temperature for a certain period of time, followed by being soft baked at 80 °C for 2 min and N_2 gas blow-drying. The LiF (≥99.9%, high purity chemicals) was dissolved in deionized water to make a LiF solution with a concentration of 0.01 M and stirred at 80 °C for 5 min. The DUV light with a wavelength of 220 nm and an average intensity of 11 mW cm^{-2} was used to measure the photoresponse of the devices under vacuum at room temperature.

3. RESULTS AND DISCUSSION

Figure 1a shows the schematic of an ML-WS_2 back gate FET. The source−drain contacts (Cr/Au thickness of 8/60 nm) for ML-WS_2 were made employing e-beam lithography. An optical image of the device is shown in Figure 1b. The thickness of WS_2 nanoflakes were further confirmed by AFM. Figure 1c shows the surface topologies of the WS_2 flakes taken by tapping mode of AFM under ambient conditions. In Figure 1d, the thickness of the WS_2 flake is about 5.2 nm, which correspond to multilayer WS_2.

To check the device performance, the electrical properties were measured before and after doping in vacuum at room temperature. Figure 2a shows the transfer characteristics of the as-made device at a fixed drain−source voltage (V_{ds} = 1 V) with a channel length of 0.5 μm. The low off-state current (10^{-11} at V_{ds} = 1 V) is observed due to the relatively large band gap and ultrathin body nature of WS_2 FETs, which is good for low power nanoelectronic devices. The device exhibits a typical switching behavior with a current on/off ratio of 4.83×10^5 and a threshold voltage of 14 V, which is calculated by linear extrapolation of $I_{ds}-V_{bg}$ curves. After doping with LiF, the current on/off ratio has been increased 2-fold due to the improvement of the on current, and the threshold voltage is

DOI: 10.1021/acsami.5b06825
ACS Appl. Mater. Interfaces XXXX, XXX, XXX−XXX

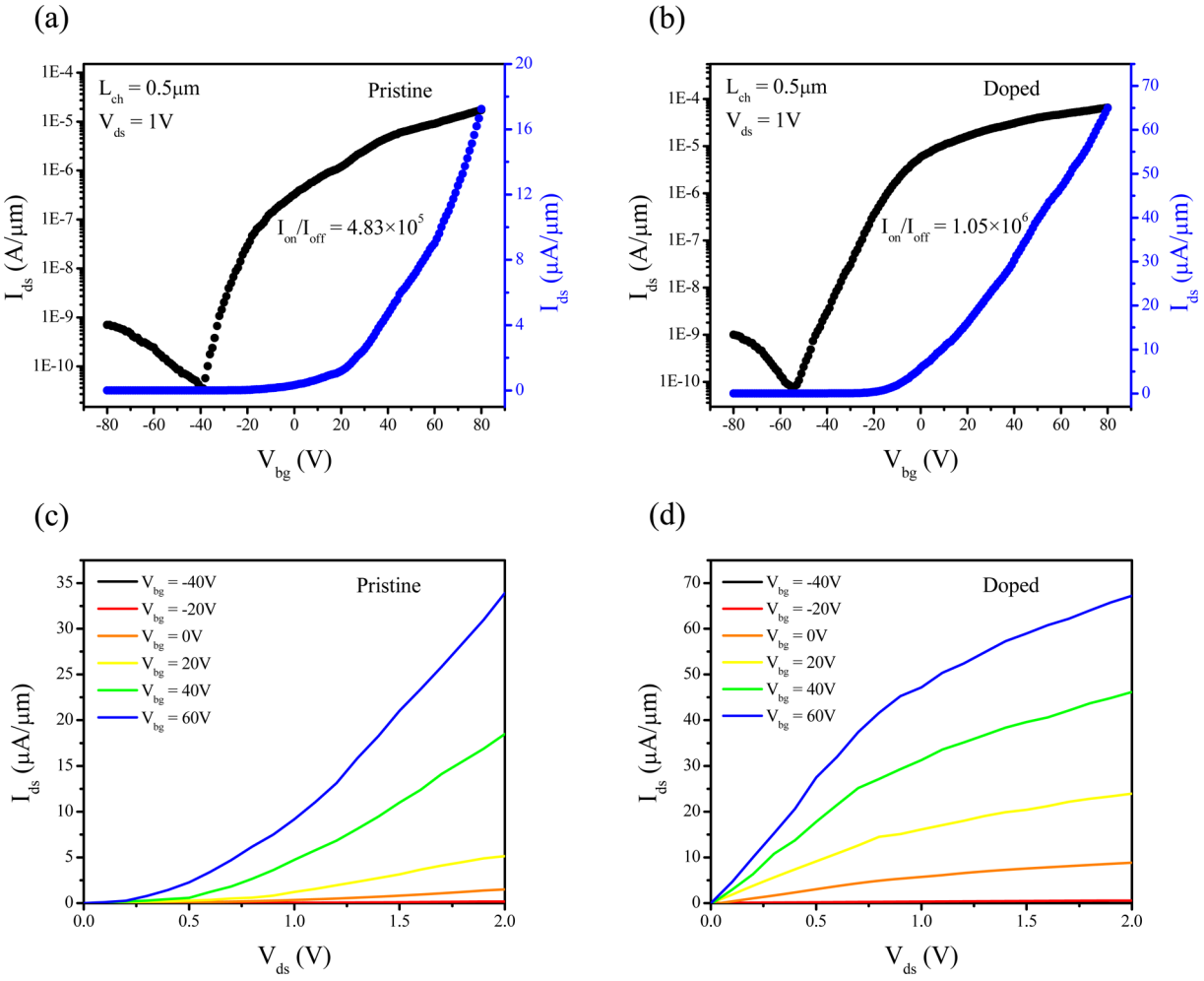

Figure 2. (a) Transfer characteristic of the pristine ML-WS_2 FET device with a channel length of 0.5 μm at V_{ds} = 1 V plotted in log scale (left vertical axis) and linear scale (right vertical axis). The on/off ratio of the pristine device is 4.83×10^5. (b) Transfer characteristics of the LiF-doped ML-WS_2 FET device. The on/off ratio of the doped device is 1.05×10^6. (c) Output characteristics of the pristine device shown in (a). The nonlinear output characteristics suggest the existence of a large Schottky barrier, which limits the drain current. (d) Output characteristics of the doped device shown in (b). The drain current is normalized to the width of the sample.

shifted from 14 to −6 V, shown in Figure 2b. The negative shift of threshold voltage confirms n-doping in the channel (Supporting Information: transfer characteristics for different channel lengths). The output characteristics of the pristine and doped ML-WS_2 FETs with a 0.5 μm channel length are shown in Figure 2c,d. The nonlinear output characteristics in Figure 2c suggest the existence of a considerable level of Schottky barrier in our device with Cr/Au electrodes. Compared with the undoped device, the device current of the LiF-doped ML-WS_2 has been improved by more than 4 times. The drain current is nearly saturated at high drain biases for all gate voltages. The improvement in drain current with doping is mainly due to these effects: (1) reduction in SB height with strong doping and (2) higher channel conductance arising from the increased electron concentration.[30]

To quantify the effect of WS_2 doping on the Au−WS_2 interface, we have extracted the contact resistance using TLM for doped and undoped devices. Figure 3a shows the schematic of a multiple channel length device fabricated on an ML-WS_2 FET. The transfer characteristics curves for doped and undoped devices with channel lengths varying from 0.5 to 2 μm are shown in Figure 3b. Before LiF doping, all of the devices show strong gate voltage dependence with a threshold voltage of about 14 V. After doping, the on current increases and the minimal gate bias dependence was observed. The estimated total resistance (R_{total}) of WS_2 FETs can be expressed as follows

$$R_{total} = R_{channel} + 2R_c \quad (1)$$

Here, $R_{channel}$ is the channel resistance for WS_2 and R_c is the contact resistance at metal−WS_2 junctions. The contact resistance can be extracted by linearly fitting the curve of total resistance for a given gate voltage. Figure 3c shows the TLM resistance of the doped and undoped WS_2 FTEs as a function of channel length at V_{bg} = 60 V. The R_c value after LiF doping was reduced to as low as 0.9 kΩ·μm.

The mechanism of the reduction in contact resistance can be explained with the energy band diagrams of the Au/WS_2 contacts shown in Figure 3d. The Fermi level at the Au−WS_2 interface is pinned near the charge neutrality level in the pristine case, resulting in a large Schottky barrier height (SBH). The SBH can be expressed as follows[31]

$$R_{contact} \propto \frac{1}{n} e^{(\phi_{SB}/KT)} \quad (2)$$

DOI: 10.1021/acsami.5b06825
ACS Appl. Mater. Interfaces XXXX, XXX, XXX−XXX

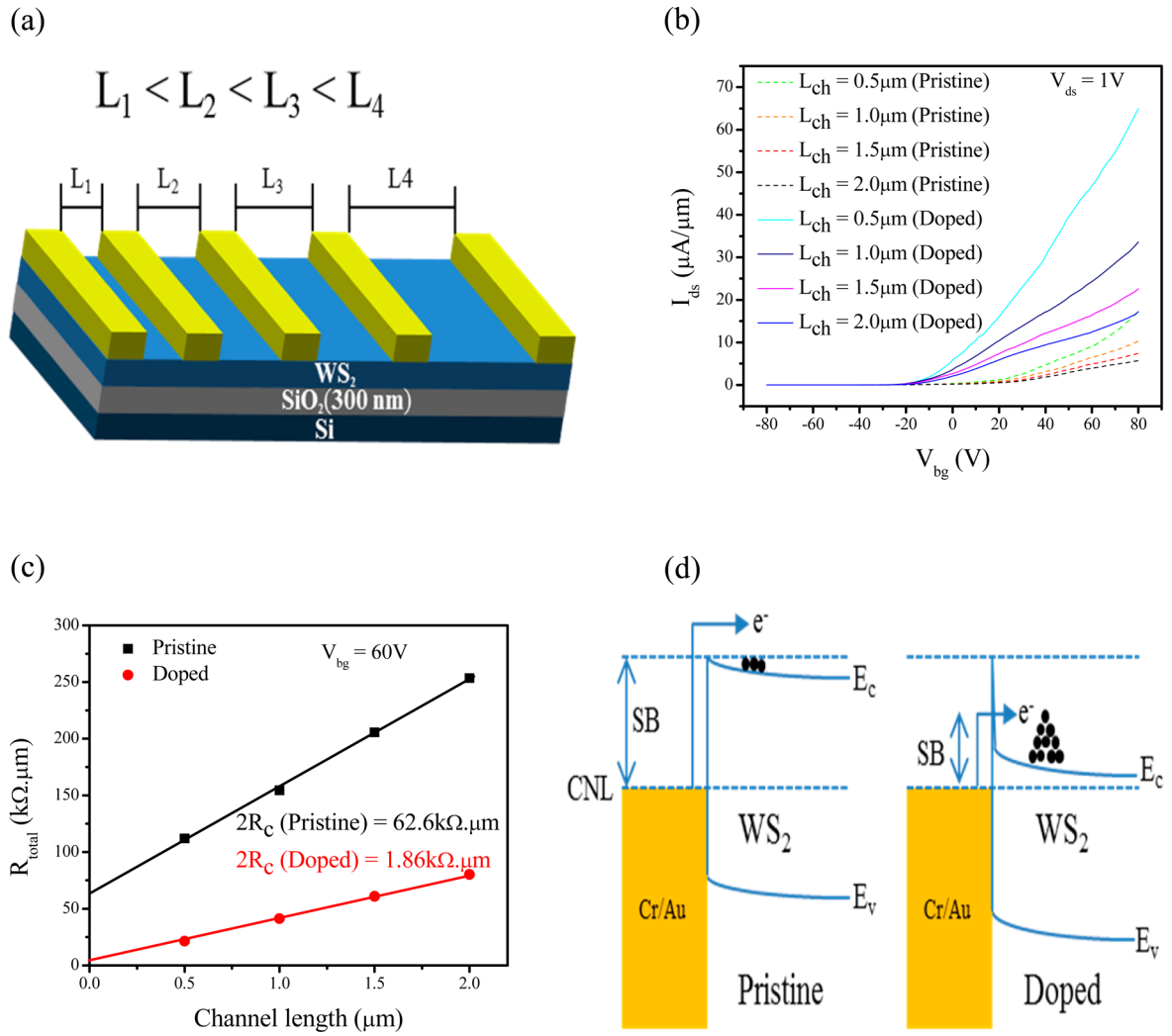

Figure 3. (a) Schematic of multiple channel length device fabricated on ML-WS_2 flake to extract the contact resistance using the transfer length method. (b) Transfer characteristics curves of the ML-WS_2 device before (dashed lines) and after (solid lines) doping with different channel lengths at V_{ds} = 1 V. (c) Total resistance as a function of channel length for pristine (black curve) and doped (red curve) samples at V_{bg} = 60 V. The contact resistance is extracted to be 0.9 kΩ·μm after LiF doping. (d) Schematic band alignment diagrams at the Au/WS_2 junctions for pristine and doped samples. Before doping, the Fermi level is located near to the CNL, resulting in a large Schottky barrier. After doping, the WS_2 is heavily doped and electrons can easily tunnel through the barrier due to the thin Schottky barrier.

$$R_{\text{channel}} \propto \frac{1}{n} \tag{3}$$

where n is the electron concentration in WS_2, φ_{SB} is the height of SB formed at the Au–WS_2 junctions, k is the Boltzmann constant, and T is the absolute temperature. It is important to note that there are two possible interfaces to form the Schottky barrier in our transistor: (a) the interface between source/drain metal and contacted WS_2 in the vertical direction and (b) the interface between source/drain metal and channel WS_2 in the lateral direction along the edges of the metal. The vertical SBH cannot be modified because the LiF doping is applied after the patterning of electrodes. Therefore, the lateral SBH can be modulated with doping and its height is determined by the energy difference between the Fermi level of the Au and the conduction band maximum of the channel WS_2. Compared to the undoped device, it would be much easier for electrons to tunnel through the barrier because the tunneling current starts to dominate over thermionic current through metal–semiconductor junctions. As a result, the contact resistance is significantly reduced, which leads to an improvement in drain–source current and device performance.

The adjustment in threshold voltage (V_T) with LiF doping has been observed and quantitatively measured for various ML-WS_2 devices. The V_T is extracted by linear extrapolation of I_{ds}–V_{bg} curves. Figure 4a shows the transfer characteristics curves of the device (L_{ch} = 0.5 μm) with increasing LiF doping time. The threshold voltage clearly shifts toward the negative gate voltage with the LIF doping, which revealed the n-doping in the ML-WS_2 device. The source–drain current is increased drastically by an order of magnitude after LiF doping, which is clearly due to the reduction in contact resistance. Figure 4b shows the shifting of threshold voltage with the increment in doping time. Before doping, the as-made device shows n-type transport behavior. With the increase in doping time, the V_T is shifted gradually toward a negative gate voltage. The V_T changes from 14 to −6 V after 120 min of LiF doping. To further confirm the LiF doping effect on threshold voltage, all of the devices with different channel lengths have been measured before and after doping (Figure S1, Supporting Information). All devices show a

DOI: 10.1021/acsami.5b06825
ACS Appl. Mater. Interfaces XXXX, XXX, XXX–XXX

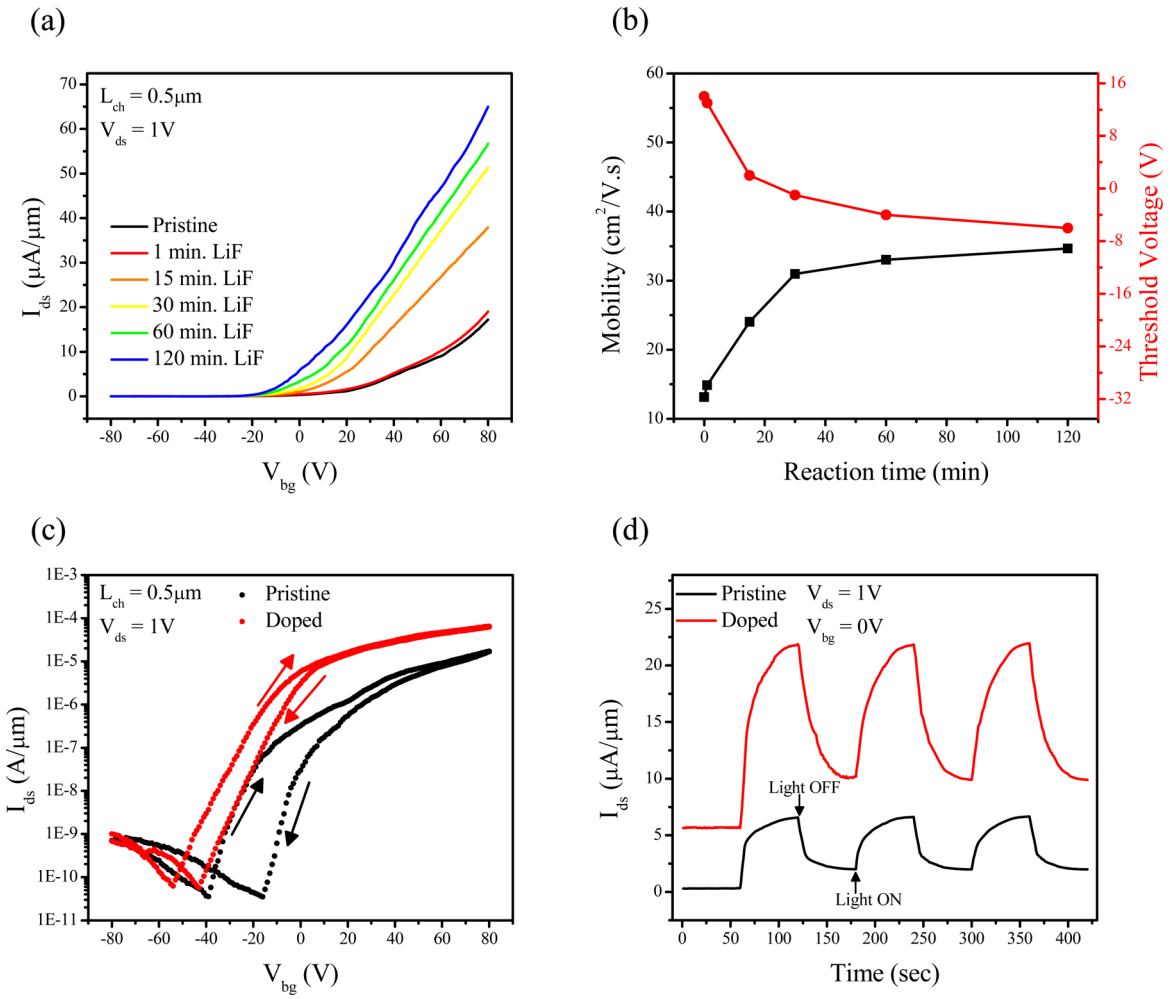

Figure 4. (a) Transfer characteristics curves of the ML-WS_2 device (L_{ch} = 0.5 μm) as a function of LiF exposure time. The black curve is for the pristine sample, while the other curves from bottom to top are after 1, 15, 30, 60, and 120 min LiF doping. The device clearly shows the effective n-doping of WS_2. (b) Electron mobility and threshold voltage as a function of different reaction times for the device shown in (a). (c) Dual sweep transfer characteristics of the doped and undoped devices with a channel length of 0.5 μm at V_{ds} = 1 V. (d) Time-dependent photocurrent response of the ML-WS_2 FET before (black curve) and after doping (red curve) under vacuum during the DUV light switching on/off. A constant source–drain voltage of 1 V was applied and measures the I_{ds} for photocurrent response.

similar negative shift in V_T after doping, which demonstrates that this doping technique could be a possible way to tune the threshold voltage in other 2D materials.

The doping mechanism on WS_2 by the LiF treatment can be understood as follows. As a member of the fourth transition group of the periodic table, tungsten (W) with a valence electronic configuration $6s^25d^4$ possess an electropositive character, showing capacity to accept electrons. Additionally, the LiF could be dissociated in electropositive Li^+ (electron acceptor) and electronegative F^- (electron donor) ions. When F^- atoms are incorporated in WS_2, they occupy the location of sulfur vacancies to generate the defects levels. These defect levels originate from the hybridization of 3p and 5d orbitals of F^- and W, respectively.[32] Thus, upon doping F^- ions in WS_2, the discrete impurity energy levels in WS_2 would emerge into the conduction band, resulting in the band gap narrowing and the degeneration doping.[33] Hence, we presumed that the n-type doping effect in WS_2 is achieved by the donation of an extra electron by F^- ions when they occupy the location of sulfur vacancies.[10]

The mobility of ML-WS_2 could also be affected by the contact resistance or Schottky barrier. The low contact resistance would enhance the output current I_{ds} and electron mobility. However, in our undoped sample, the nonlinear output characteristics (Figure 1c) suggest the existence of a Schottky barrier between Au–WS_2 contacts. Thus, there is an incredible room to improve the mobility of the ML-WS_2 device by using a chemical doping method. The mobility of the samples was extracted by using the relation

$$\mu = \frac{L}{C_g W V_{ds}} \left(\frac{dI_{ds}}{dV_g} \right) \tag{4}$$

where L is the channel length, W is the channel width, C_g is the gate capacitance (115 aF μm^{-2}) calculated for our Si/SiO_2 substrate, V_{ds} = 1 V, and $((dI_{ds})/(dV_g))$ is the slope of transfer characteristics of the device. The mobility of our undoped ML-WS_2 sample is comparable to other 2D TMD materials like MoS_2. However, after LiF doping, the field effect mobility significantly improves from 13.2 to 34.7 $cm^2/(V\ s)$ due to the improvement in source–drain current, which is shown in Figure 4b. The improvement in mobility is due to the increase in electron concentration after LiF doping, which changes the Fermi level of the WS_2 and lowers the SBH.

DOI: 10.1021/acsami.5b06825
ACS Appl. Mater. Interfaces XXXX, XXX, XXX–XXX

The asymmetry in conductivity and the hysteresis effect in transfer characteristic were observed in vacuum for ML-WS_2 FETs. Figure 4c shows the hysteresis curves for doped and undoped samples (L_{ch} = 0.5 μm), where the gate voltage was swept from −80 to 80 V and back to 80 V. The change in gate voltage sweep direction from forward to backward induces a significant shift of 23 V for the undoped sample, which is attributed to charge trapping near the WS_2 channel, i.e., in the dielectric, WS_2−oxide interface or WS_2 top surface. After LiF doping, the hysteresis was dramatically suppressed, as the change of threshold voltage in the hysteresis curve reduced to 11 V from 23 V. The reduction in hysteresis might be due to the removal of foreign impurities on the WS_2 surface after LiF doping (Supporting Information: hysteresis curves for different channel length devices).

Besides the traditional applications of TMD materials as field effect transistors and heterostrucutre junctions, films of these materials can also be used as photodetecting devices due to their large optical absorption property. The photocurrent of ML-WS_2 FETs was measured in a vacuum under illumination from the DUV light with a 220 nm wavelength. Photocurrent (I_{ph}) is defined as the difference of source−drain current with and without the illuminated light. As shown in Figure 4d, the photocurrent as a function of time was measured before and after doping under the alternative dark and illumination conditions at a fixed bias voltage of 1 V. Compared to pristine, the photocurrent is increased about 2.6 times after doping. The improvement in photocurrent was mainly due to the increment in electron mobility and charge density after doping with LiF. The similar response of photocurrent was observed for all other devices we tested.

Raman spectroscopic studies were performed to confirm the number of layers, quality of WS_2 films, and the effect of doping. Figure 5a shows that the first-order Raman spectra of WS_2 nanoflakes exhibit two optical phonon modes at approximately 355 and 420 cm^{-1}, corresponding to the in-plane E^1_{2g} (Γ) and out-of-plane A_{1g} (Γ) vibrations, respectively.[34,35] A second-order 2LA (M) mode was also observed at approximately 350 cm^{-1}. The change in the relative peak intensity ratios (E^1_{2g}/A_{1g}) and the frequency difference between the E^1_{2g} and A_{1g} modes vary with layer thickness.[34] To clarify this observation, we carried out Lorentzian curve fitting to extract the peak intensities, positions, and full width at half-maximum (fwhm) of E^1_{2g} and A_{1g} and 2LA modes and show the results in Figure 5b. The peak spacing between A_{1g} and E^1_{2g} modes ($\Delta = A_{1g} - E^1_{2g}$) is about 65.4, which indicates an ML-WS_2 film. The energy difference between the A_{1g} and 2LA (M) and the relative peak intensity ratio of I_{2LA}/I_{A1g} modes are about 70.3 cm^{-1} and 0.43, also confirming the ML-WS_2 films.[34,36] Our Raman results for ML-WS_2 films agree well with those in the previous reports.[30,34,37] The chemically doped samples were also characterized by Raman spectroscopy. Figure 5a shows the Raman spectra of pristine and doped ML-WS_2 films. After doping with LiF, both A_{1g} and E^1_{2g} peaks shifted to a lower wavenumber, thus indicating the n-doping. Furthermore, the fwhm of both A_{1g} and E^1_{2g} peaks showed broadening after doping. These spectroscopic results are comparable to those in previous reports.[34,38]

The long-term stability of the doping of 2D materials is still a big challenge nowadays. We, therefore, check the stability of our doped sample after 2 weeks in an atmospheric environment. In Figure 6a, we show the transfer characteristics of the freshly doped ML-WS_2 device and the device after the 2 weeks

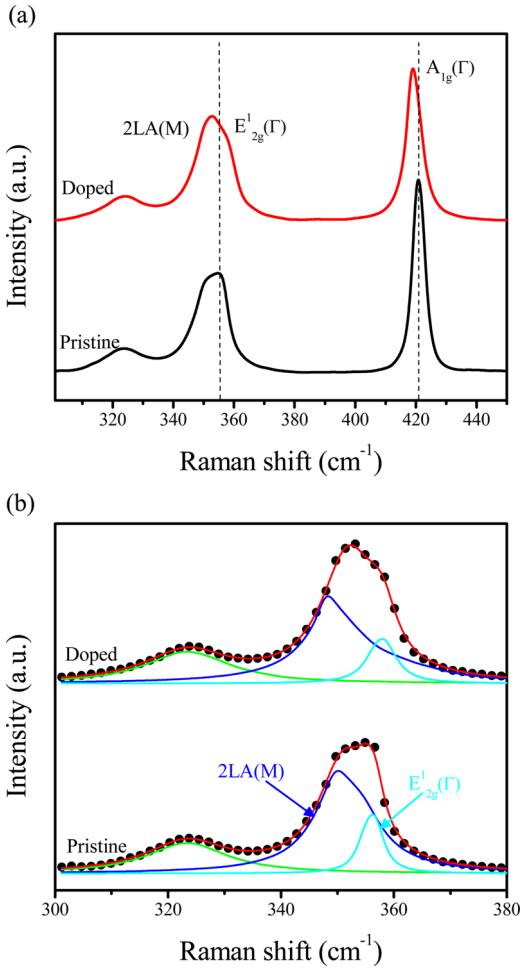

Figure 5. (a) Room-temperature Raman spectra of an ML-WS_2 flake before (black curve) and after (red curve) doping using the 514 nm laser. (b) Lorentzian curve fit for E^1_{2g} and 2LA (M) peaks. Black circles represent the experimental data; blue, cyan, and red lines represent the 2LA (M), E^1_{2g}, and combined peak fitting, respectively.

of initial measurements. Except for a minor change in output current, the transfer characteristics of the device after 2 weeks remain the same as the fresh one. Figure 6b shows the TLM resistance of the ML-WS_2 film for freshly doped and the device after 2 weeks of initial measurement. The contact resistance was slightly increased from 0.9 to 1.3 kΩ·μm, which indicates that our doped devices are very stable.

4. CONCLUSION

We have demonstrated a highly stable doping method using LIF as dopant source to improve the electrical and photoelectrical properties of WS_2 FETs. The contact resistance of our doped device has been reduced to 0.9 kΩ·μm due to the n-type doping with LiF, thus the reduction in Schottky barrier width. Electrical and Raman studies were also performed to confirm the improvement in charge carrier mobility, on/off ratio, drain current, and photocurrent response. The 0.5 μm WS_2 FET has performed as n-type behavior after doping with a high drain current of 65 μA/μm, a high on/off ratio of 1.05 × 10^6, and an electron mobility of around 34 $cm^2/(V\ s)$. Moreover, this doping technique also enhanced the photocurrent in WS_2 FETs. Our results demonstrate that this doping technique can also be applied to other TMD materials to reduce the

DOI: 10.1021/acsami.5b06825
ACS Appl. Mater. Interfaces XXXX, XXX, XXX−XXX

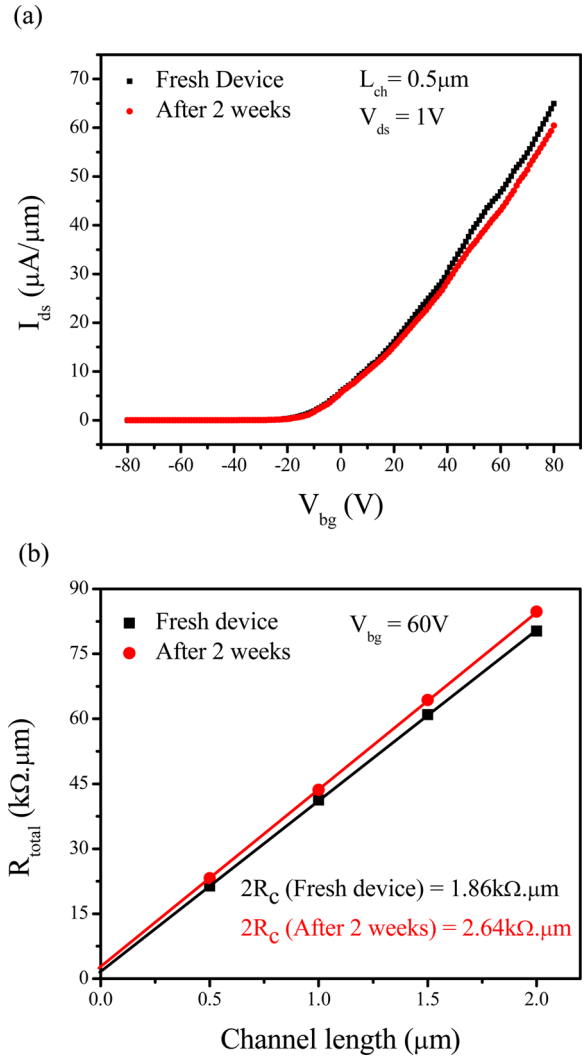

Figure 6. (a) Transfer characteristics curves of the freshly doped (black curve) ML-WS_2 FET with a channel length of 0.5 μm and after 2 weeks of initial doping (red curve). (b) Total resistance versus channel length of the freshly doped device (black curve) and after 2 weeks of initial doping (red curve) at V_{bg} = 60 V.

contact resistance and probe the intrinsic properties of the materials.

■ ASSOCIATED CONTENT

Supporting Information

The Supporting Information is available free of charge on the ACS Publications website at DOI: 10.1021/acsami.5b06825.

Transfer characteristics of the pristine and doped ML-WS_2 FET devices and the dual sweep transfer characteristics of the pristine and doped devices with different channel lengths (PDF)

■ AUTHOR INFORMATION

Corresponding Author

*E-mail: hnoh@sejong.ac.kr. Tel: +82-2-3408-3986.

Notes

The authors declare no competing financial interest.

■ ACKNOWLEDGMENTS

This research was supported by the Basic Science Research Program through the National Research Foundation of Korea (NRF) funded by the Ministry of Education (2010-0020207) and (2014R1A1A2055503).

■ REFERENCES

(1) Geim, A. K. Graphene: Status and Prospects. *Science* **2009**, *324*, 1530−1534.
(2) Avouris, P.; Chen, Z. H.; Perebeinos, V. Carbon-Based Electronics. *Nat. Nanotechnol.* **2007**, *2*, 605−615.
(3) Schwierz, F. Graphene Transistors. *Nat. Nanotechnol.* **2010**, *5*, 487−496.
(4) Elias, D. C.; Gorbachev, R. V.; Mayorov, A. S.; Morozov, S. V.; Zhukov, A. A.; Blake, P.; Ponomarenko, L. A.; Grigorieva, I. V.; Novoselov, K. S.; Guinea, F.; Geim, A. K. Dirac Cones Reshaped by Interaction Effects in Suspended Graphene. *Nat. Phys.* **2011**, *7*, 701−704.
(5) Geim, A. K.; Novoselov, K. S. The Rise of Graphene. *Nat. Mater.* **2007**, *6*, 183−191.
(6) Wilson, J. A.; Yoffe, A. D. The Transition Metal Dichalcogenides Discussion and Interpretation of the Observed Optical, Electrical and Structural Properties. *Adv. Phys.* **1969**, *18*, 193−335.
(7) Yoffe, A. D. Layer Compounds. *Annu. Rev. Mater. Sci.* **1973**, *3*, 147−170.
(8) Radisavljevic, B.; Kis, A. Mobility Engineering and a Metal-Insulator Transition in Monolayer MoS_2. *Nat. Mater.* **2013**, *12*, 815−820.
(9) Bao, W. Z.; Cai, X. H.; Kim, D.; Sridhara, K.; Fuhrer, M. S. High Mobility Ambipolar MoS_2 Field-Effect Transistors: Substrate and Dielectric Effects. *Appl. Phys. Lett.* **2013**, *102*, 042104.
(10) Yang, L. M.; Majumdar, K.; Liu, H.; Du, Y. C.; Wu, H.; Hatzistergos, M.; Hung, P. Y.; Tieckelmann, R.; Tsai, W.; Hobbs, C.; Ye, P. D. Chloride Molecular Doping Technique on 2D Materials: WS_2 and MoS_2. *Nano Lett.* **2014**, *14*, 6275−6280.
(11) Iqbal, M. W.; Iqbal, M. Z.; Khan, M. F.; Shehzad, M. A.; Seo, Y.; Park, J. H.; Hwang, C.; Eom, J. High-Mobility and Air-Stable Single-Layer WS_2 Field-Effect Transistors Sandwiched Between Chemical Vapor Deposition-Grown Hexagonal BN Films. *Sci. Rep.* **2015**, *5*, 10699.
(12) Jena, D.; Konar, A. Enhancement of Carrier Mobility in Semiconductor Nanostructures by Dielectric Engineering. *Phys. Rev. Lett.* **2007**, *98*, 136805.
(13) Walia, S.; Balendhran, S.; Wang, Y. C.; Ab Kadir, R.; Zoolfakar, A. S.; Atkin, P.; Ou, J. Z.; Sriram, S.; Kalantar-zadeh, K.; Bhaskaran, M. Characterization of Metal Contacts for Two-Dimensional MoS_2 Nanoflakes. *Appl. Phys. Lett.* **2013**, *103*, 232105.
(14) Das, S.; Chen, H. Y.; Penumatcha, A. V.; Appenzeller, J. High Performance Multilayer MoS_2 Transistors with Scandium Contacts. *Nano Lett.* **2013**, *13*, 100−105.
(15) Chen, J. R.; Odenthal, P. M.; Swartz, A. G.; Floyd, G. C.; Wen, H.; Luo, K. Y.; Kawakami, R. K. Control of Schottky Barriers in Single Layer MoS_2 Transistors with Ferromagnetic Contacts. *Nano Lett.* **2013**, *13*, 3106−3110.
(16) Dankert, A.; Langouche, L.; Kamalakar, M. V.; Dash, S. P. High-Performance Molybdenum Disulfide Field-Effect Transistors with Spin Tunnel Contacts. *ACS Nano* **2014**, *8*, 476−482.
(17) Chuang, S.; Battaglia, C.; Azcatl, A.; McDonnell, S.; Kang, J. S.; Yin, X. T.; Tosun, M.; Kapadia, R.; Fang, H.; Wallace, R. M.; Javey, A. MoS_2 P-type Transistors and Diodes Enabled by High Work Function MoO_x Contacts. *Nano Lett.* **2014**, *14*, 1337−1342.
(18) Jariwala, D.; Sangwan, V. K.; Late, D. J.; Johns, J. E.; Dravid, V. P.; Marks, T. J.; Lauhon, L. J.; Hersam, M. C. Band-Like Transport in High Mobility Unencapsulated Single-Layer MoS_2 Transistors. *Appl. Phys. Lett.* **2013**, *102*, 173107.
(19) Lin, J. H.; Cretu, O.; Zhou, W.; Suenaga, K.; Prasai, D.; Bolotin, K. I.; Cuong, N. T.; Otani, M.; Okada, S.; Lupini, A. R.; Idrobo, J. C.; Caudel, D.; Burger, A.; Ghimire, N. J.; Yan, J. Q.; Mandrus, D. G.;

DOI: 10.1021/acsami.5b06825
ACS Appl. Mater. Interfaces XXXX, XXX, XXX−XXX

Pennycook, S. J.; Pantelides, S. T. Flexible Metallic Nanowires with Self-Adaptive Contacts to Semiconducting Transition-Metal Dichalcogenide Monolayers. *Nat. Nanotechnol.* **2014**, *9*, 436−442.
(20) Liu, W.; Kang, J. H.; Sarkar, D.; Khatami, Y.; Jena, D.; Banerjee, K. Role of Metal Contacts in Designing High-Performance Monolayer N-Type WSe_2 Field Effect Transistors. *Nano Lett.* **2013**, *13*, 1983−1990.
(21) Larentis, S.; Fallahazad, B.; Tutuc, E. Field-Effect Transistors and Intrinsic Mobility in Ultra-Thin $MoSe_2$ Layers. *Appl. Phys. Lett.* **2012**, *101*, 223104.
(22) Liu, H.; Neal, A. T.; Du, Y.; Ye, P. D. Fundamentals in MoS_2 Transistors: Dielectric, Scaling and Metal Contacts. *ECS Trans.* **2013**, *58*, 203−208.
(23) Kang, J. H.; Liu, W.; Banerjee, K. High-Performance MoS_2 Transistors with Low-Resistance Molybdenum Contacts. *Appl. Phys. Lett.* **2014**, *104*, 093106.
(24) Radisavljevic, B.; Radenovic, A.; Brivio, J.; Giacometti, V.; Kis, A. Single-Layer MoS_2 Transistors. *Nat. Nanotechnol.* **2011**, *6*, 147−150.
(25) Kang, J.; Tongay, S.; Zhou, J.; Li, J. B.; Wu, J. Q. Band Offsets and Heterostructures of Two-Dimensional Semiconductors. *Appl. Phys. Lett.* **2013**, *102*, 012111.
(26) Gong, C.; Zhang, H. J.; Wang, W. H.; Colombo, L.; Wallace, R. M.; Cho, K. J. Band Alignment of Two-Dimensional Transition Metal Dichalcogenides: Application in Tunnel Field Effect Transistors. *Appl. Phys. Lett.* **2013**, *103*, 053513.
(27) Yu, A. Y. C. Electron Tunneling and Contact Resistance of Metal-Silicon Contact Barriers. *Solid-State Electron.* **1970**, *13*, 239−247.
(28) Du, Y. C.; Liu, H.; Neal, A. T.; Si, M. W.; Ye, P. D. Molecular Doping of Multilayer MoS_2 Field-Effect Transistors: Reduction in Sheet and Contact Resistances. *IEEE Electron Device Lett.* **2013**, *34*, 1328−1330.
(29) Fang, H.; Tosun, M.; Seol, G.; Chang, T. C.; Takei, K.; Guo, J.; Javey, A. Degenerate N-Doping of Few-Layer Transition Metal Dichalcogenides by Potassium. *Nano Lett.* **2013**, *13*, 1991−1995.
(30) Iqbal, M. W.; Iqbal, M. Z.; Khan, M. F.; Shehzad, M. A.; Seo, Y.; Eom, J. Deep-Ultraviolet-Light-Driven Reversible Doping of WS_2 Field-Effect Transistors. *Nanoscale* **2015**, *7*, 747−757.
(31) Liu, B. L.; Chen, L.; Liu, G.; Abbas, A. N.; Fathi, M.; Zhou, C. W. High-Performance Chemical Sensing Using Schottky-Contacted Chemical Vapor Deposition Grown Mono Layer MoS_2 Transistors. *ACS Nano* **2014**, *8*, 5304−5314.
(32) Dolui, K.; Rungger, I.; Das Pemmaraju, C.; Sanvito, S. Possible Doping Strategies for MoS_2 Monolayers: An Ab Initio Study. *Phys. Rev. B: Condens. Matter Mater. Phys.* **2013**, *88*, 075420.
(33) Sun, Q. Q.; Li, Y. J.; He, J. L.; Yang, W.; Zhou, P.; Lu, H. L.; Ding, S. J.; Zhang, D. W. The Physics and Backward Diode Behavior of Heavily Doped Single Layer MoS_2 Based P-N Junctions. *Appl. Phys. Lett.* **2013**, *102*, 093104.
(34) Berkdemir, A.; Gutierrez, H. R.; Botello-Mendez, A. R.; Perea-Lopez, N.; Elias, A. L.; Chia, C. I.; Wang, B.; Crespi, V. H.; Lopez-Urias, F.; Charlier, J. C.; Terrones, H.; Terrones, M. Identification of Individual and Few Layers of WS_2 using Raman Spectroscopy. *Sci. Rep.* **2013**, *3*, 1755.
(35) Elias, A. L.; Perea-Lopez, N.; Castro-Beltran, A.; Berkdemir, A.; Lv, R. T.; Feng, S. M.; Long, A. D.; Hayashi, T.; Kim, Y. A.; Endo, M.; Gutierrez, H. R.; Pradhan, N. R.; Balicas, L.; Mallouk, T. E.; Lopez-Urias, F.; Terrones, H.; Terrones, M. Controlled Synthesis and Transfer of Large-Area WS_2 Sheets: From Single Layer to Few Layers. *ACS Nano* **2013**, *7*, 5235−5242.
(36) Zeng, H. L.; Liu, G. B.; Dai, J. F.; Yan, Y. J.; Zhu, B. R.; He, R. C.; Xie, L.; Xu, S. J.; Chen, X. H.; Yao, W.; Cui, X. D. Optical Signature of Symmetry Variations and Spin-Valley Coupling in Atomically Thin Tungsten Dichalcogenides. *Sci. Rep.* **2013**, *3*, 1608.
(37) Zhao, W. J.; Ghorannevis, Z.; Amara, K. K.; Pang, J. R.; Toh, M.; Zhang, X.; Kloc, C.; Tan, P. H.; Eda, G. Lattice Dynamics in Mono- and Few-Layer Sheets of WS_2 and WSe_2. *Nanoscale* **2013**, *5*, 9677−9683.
(38) Kiriya, D.; Tosun, M.; Zhao, P. D.; Kang, J. S.; Javey, A. Air-Stable Surface Charge Transfer Doping of MoS_2 by Benzyl Viologen. *J. Am. Chem. Soc.* **2014**, *136*, 7853−7856.

DOI: 10.1021/acsami.5b06825
ACS Appl. Mater. Interfaces XXXX, XXX, XXX−XXX